This article was downloaded by: [National Chiao Tung University 國立交通大學]
On: 26 April 2014, At: 00:37
Publisher: Taylor & Francis
Informa Ltd Registered in England and Wales Registered Number: 1072954 Registered office: Mortimer House, 37-41 Mortimer Street, London W1T 3JH, UK

Aerosol Science and Technology
Publication details, including instructions for authors and subscription information:
http://www.tandfonline.com/loi/uast20

Continuous Generation of TiO_2 Nanoparticles by an Atmospheric Pressure Plasma-Enhanced Process

Chienchih Chen [a], Hsunling Bai [a], HungMin Chein [b] & Tzu Ming Chen [b]
[a] Institute of Environmental Engineering, National Chiao Tung University, Hsinchu, Taiwan
[b] Energy and Environment Research Laboratories, Industrial Technology Research Institute, Hsinchu, Taiwan
Published online: 06 Nov 2007.

To cite this article: Chienchih Chen, Hsunling Bai, HungMin Chein & Tzu Ming Chen (2007) Continuous Generation of TiO_2 Nanoparticles by an Atmospheric Pressure Plasma-Enhanced Process, Aerosol Science and Technology, 41:11, 1018-1028, DOI: 10.1080/02786820701694355

To link to this article: http://dx.doi.org/10.1080/02786820701694355

PLEASE SCROLL DOWN FOR ARTICLE

Taylor & Francis makes every effort to ensure the accuracy of all the information (the "Content") contained in the publications on our platform. However, Taylor & Francis, our agents, and our licensors make no representations or warranties whatsoever as to the accuracy, completeness, or suitability for any purpose of the Content. Any opinions and views expressed in this publication are the opinions and views of the authors, and are not the views of or endorsed by Taylor & Francis. The accuracy of the Content should not be relied upon and should be independently verified with primary sources of information. Taylor and Francis shall not be liable for any losses, actions, claims, proceedings, demands, costs, expenses, damages, and other liabilities whatsoever or howsoever caused arising directly or indirectly in connection with, in relation to or arising out of the use of the Content.

This article may be used for research, teaching, and private study purposes. Any substantial or systematic reproduction, redistribution, reselling, loan, sub-licensing, systematic supply, or distribution in any form to anyone is expressly forbidden. Terms & Conditions of access and use can be found at http://www.tandfonline.com/page/terms-and-conditions

Aerosol Science and Technology, 41:1018–1028, 2007
Copyright © American Association for Aerosol Research
ISSN: 0278-6826 print / 1521-7388 online
DOI: 10.1080/02786820701694355

Continuous Generation of TiO_2 Nanoparticles by an Atmospheric Pressure Plasma-Enhanced Process

Chienchih Chen,[1] Hsunling Bai,[1] HungMin Chein,[2] and Tzu Ming Chen[2]

[1]*Institute of Environmental Engineering, National Chiao Tung University, Hsinchu, Taiwan*
[2]*Energy and Environment Research Laboratories, Industrial Technology Research Institute, Hsinchu, Taiwan*

Downloaded by [National Chiao Tung University] at 00:37 26 April 2014

A novel method for the continuous generation of titanium dioxide (TiO_2) nanoparticles by dielectric barrier discharge process is presented using titanium tetraisopropoxide (TTIP) and water as precursors. The aerosol generator employs an atmospheric pressure plasma enhanced nanoparticle synthesis (APPENS) process of alternative current (AC). The influences of applied voltage, frequency and precursor molar ratio on the generated particles were described by the SEM, XRD, and SMPS analyses. The results showed that TiO_2 particles appear to be in a broad size range of bi-modal distribution when no voltage is applied. While after applying the AC plasma they become uni-modal distributed with average sizes range from around 30 to 60 nm. The applied electric frequency can be adjusted to either generate nanoparticles after the plasma reactor or develop a thin film in the reactor. An increase in the precursor molar ratio leads larger particles with a broader size distribution.

1. INTRODUCTION

The TiO_2 nanoparticles have attracted many studies on their potential applications including photocatalytic destruction of various environmental pollutants, photocatalytic sterilization, photocatalytic cancer treatment, antifogging, self-cleaning, and solar cell materials (Fujishima et al. 2000; Hoffmann et al. 1995; Nakada et al. 2002). In addition to the wide application of TiO_2 nanoparticles, their implications on human health and biological impact are also of concerns. For the purposes of studying whether on the application or implication of TiO_2 nanoparticles, the continuous production of size controllable nanoparticles is demanded.

Most of the aerosol generators are approached by physical processes where the chemical composition of generated particles is the same as the precursors. For example, the vibrating orifice (Berglund and Liu 1973), evaporation-condensation aerosol generator (Veranth et al. 2003; Peineke et al. 2006), spray (Chein and Lundgren 1995) or electrospray (Chen et al. 1995) aerosol generator, modified fluidized bed (Prenni et al. 2000), gas-metal arc welding of steels (Zimmer et al. 2002), and the spark discharge particle generator (Harvath and Gangl 2003; Evans et al. 2003). The species of physically generated particles are subjected to their dissolubility or evaporation properties.

On the contrary, the chemical process in which the chemical composition of generated particles is different from the precursors is widely applied for the production of semiconductor materials, e.g., flame synthesis (Almquist and Biswas 2002; Arabi-Katbi et al. 2001; Lee and Choi 2002; Pratsinis et al. 1996; Tsantilis et al. 2002; Wang et al. 2001; Yang et al. 1996), chemical vapor deposition (Kim et al. 2005; Nakaso et al. 2003; Park et al. 2001), thermo decomposition furnace aerosol reactor (Cho and Biswas 2006; Nakaso et al. 2001; Okuyama et al. 1986; Spicer et al. 2002; Tsantilis and Pratsinis 2004a), and plasma process (Kim et al. 2003). However, the chemical methods have not been utilized as an aerosol generator due to either their high temperature or vacuum operation condition.

The atmospheric pressure plasma of dielectric barrier discharge (DBD) was developed for ozone production by Siemens in 1852. It has also been applied to the air pollutant removals (Chang et al. 1992; Lin and Bai 2001), surface treatment (Thyen et al. 1997), and the SiO_2 thin film deposition (Foest et al. 2003; Martin et al. 2004). The atmospheric pressure plasma has also been utilized for enhancing the capture of ultra-fine particles (Kulkarni et al. 2002). In the authors' previous studies, uniform N-doped TiO_2 particles were generated by the DBD technology and successfully acted as visible light photocatalysts, it was denoted as the Atmospheric Pressure Plasma Enhanced Nanoparticle Synthesis (APPENS) process (Bai et al. 2004; Chen et al. 2007). However, the effects of the operation parameters on the generated particle size distribution have not been investigated and therefore their potential as a continuous aerosol generator has not been clarified.

Received 8 February 2007; accepted 20 September 2007.
Hsunling Bai and Chienchih Chen acknowledge the support of National Science Council, Taiwan through grant numbers NSC 93-2211-E-009-018 and NSC 94-2211-E-009-004.
Address correspondence to H. Bai, Institute of Environmental Engineering, National Chiao Tung University, 75 Po-Ai Street, Hsinchu, 300 Taiwan. E-mail: hlbai@mail.nctu.edu.tw

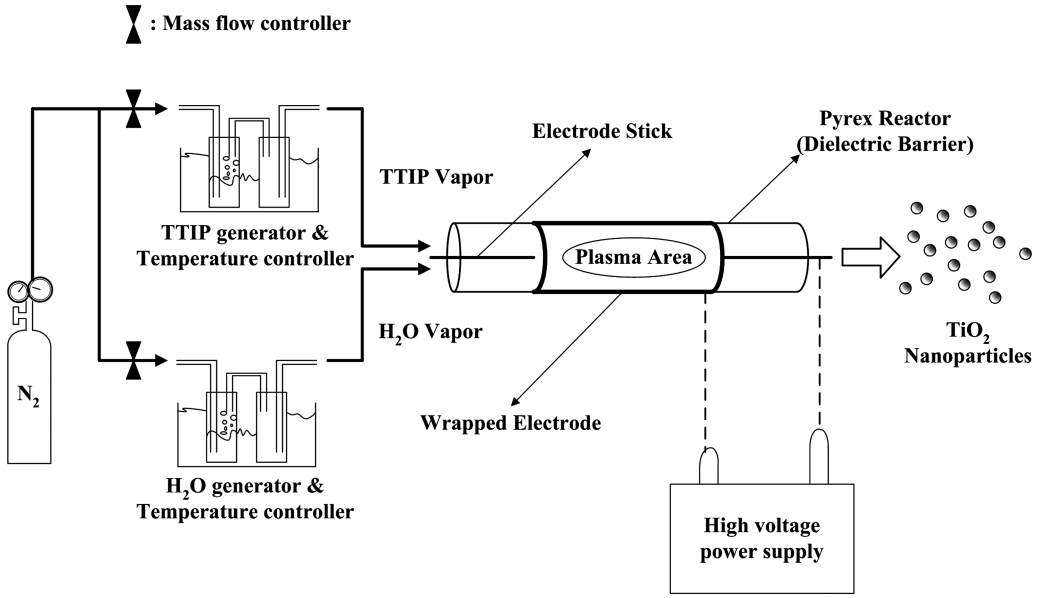

FIG. 1. Schematic diagram of APPENS reactor for producing TiO_2 nanoparticles.

Downloaded by [National Chiao Tung University] at 00:37 26 April 2014

In this study, the operation parameters of APPENS process which may influence the particle morphology, sizes, and distributions are studied. These include the applied voltage, frequency, and the precursor molar ratio employed in the APPENS process. And possibility of the process as a chemical-approached aerosol generator for the continuous generation of TiO_2 nanoparticles (<100 nm) is demonstrated.

2. EXPERIMENTAL METHOD

The APPENS process for generating TiO_2 nanoparticles is sketched in Figure 1. The aerosol reactor was a wire-tube type DBD reactor operated at atmospheric pressure and low temperature conditions. Titanium tetraisopropoxide (TTIP, $Ti(OC_3H_7)_4$) and H_2O were used as the precursor solutions for generating TiO_2 nanoparticles in this study. The precursors were vaporized and sent into the plasma reactor via passing the carrier gas through two series of impingers, they were controlled at temperatures of 150–200°C and 25°C, respectively for TTIP and water. The carrier gas was N_2 with flow rates being controlled by mass flow controllers (Brooks, 5860E), and the total flow rate of precursor vapors was 137.4 sccm. The plasma reactor was made of Pyrex glass with 21 mm I.D., 23 mm O.D., and 200 mm in length. One electrode was a stainless steel rod of 2 mm in diameter positioned along the central line of the reactor. The other electrode was a sheet of stainless steel mesh wrapped around the reactor with wrapping length of 135 mm.

The applied voltage, frequency and the precursor molar ratio were the controlling factors of particle size distribution generated by the APPENS process. The applied voltage was adjusted at the range of 0–10.20 kV, the frequency of alternative current (AC) was either 60, 120, or 240 Hz, and the precursor molar ratio was controlled by TTIP/H_2O volumetric flow rate ratio of 0.125 to 8. The corresponded TTIP/H_2O molar ratios were calculated from the vapor pressure of TTIP and H_2O to be 0.4 to 76.1 based on the equilibrium equation (Duminica et al. 2004) at a certain TTIP bubbling temperature,

$$\log P_{TTIP}(\text{Torr}) = 9.465 - \frac{3222}{T(K)},$$

where P_{TTIP} is the TTIP vapor pressure (Torr), and T is the TTIP bubbling temperature (°K).

The nanoparticles deposited on the reactor wall were collected for further analyses by SEM (Scanning Electron Microscope; HITACHI S4700) and XRPD (X-ray Powder Diffractometer; Rigaku; Cu target, 30 kV, 20 mA). The geometric mean diameter (Dp_g) and geometric standard deviation (σ_g), were determined based on averaging over 80 particles as observed from the SEM images. And for on-line measurement of particle size distribution, a SMPS (Scanning Mobility Particle Sizer, TSI model 3080L) was connected after the APPENS reactor to determine the Dp_g, σ_g, and the total mass concentration (TMC) of generated particles. In order to achieve the minimum required flow rate of the SMPS, a N_2 dilution gas stream was introduced after the plasma reactor with a N_2/aerosol dilution flow rate ratio of 1.0 (i.e., the inlet flow rate to the SMPS is double of the reactor outlet flow rate). And to further prevent agglomeration of the TiO_2 particles, a N_2/aerosol dilution flow rate ratio of 12.0 was sometimes introduced (i.e., the inlet flow rate to the SMPS is 13 times of the reactor outlet flow rate).

Downloaded by [National Chiao Tung University] at 00:37 26 April 2014

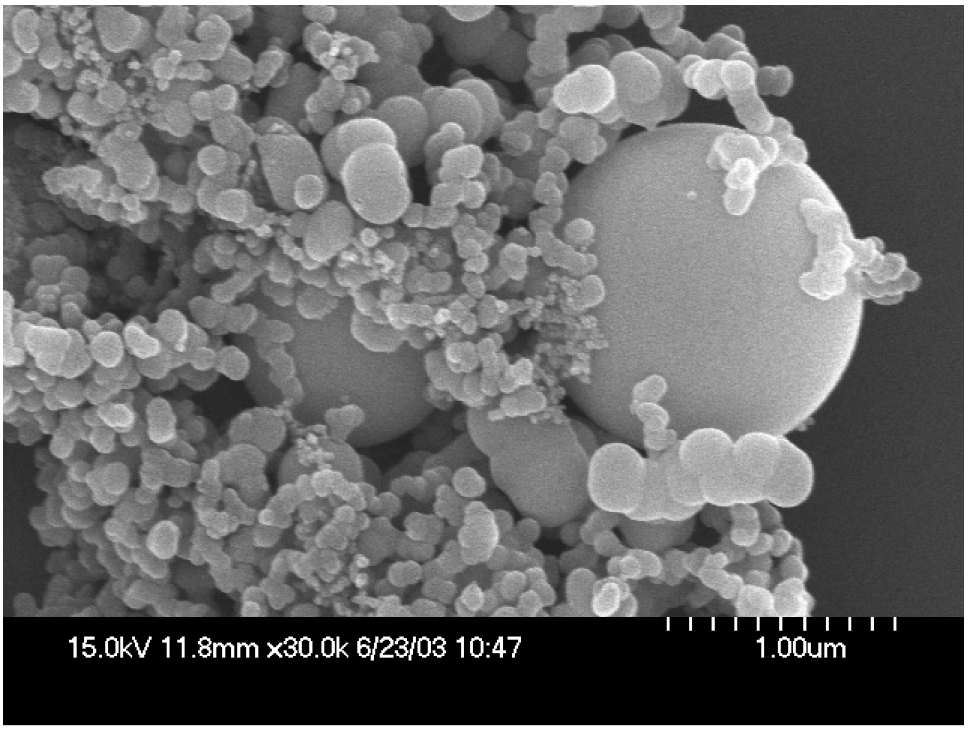

(a)

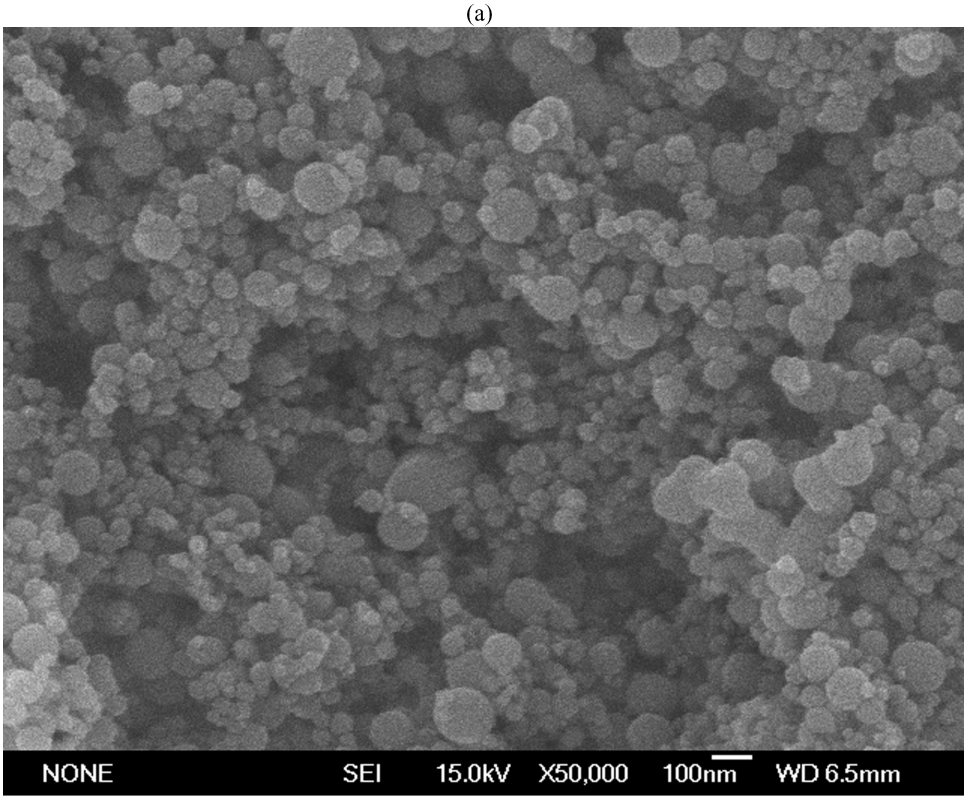

(b)

FIG. 2. SEM images of TiO_2 particles collected in the reactor under different values of applied voltage. (a) No applied voltage. (b) 6.48 kV. (c) 8.58 kV. (d) 9.60 kV. The frequency was 60 Hz, the TTIP/H_2O precursors molar ratio was 11.9 as TTIP bubbled at 150°C. The scale bar in the SEM photo is 1 μm. (*Continued*)

Downloaded by [National Chiao Tung University] at 00:37 26 April 2014

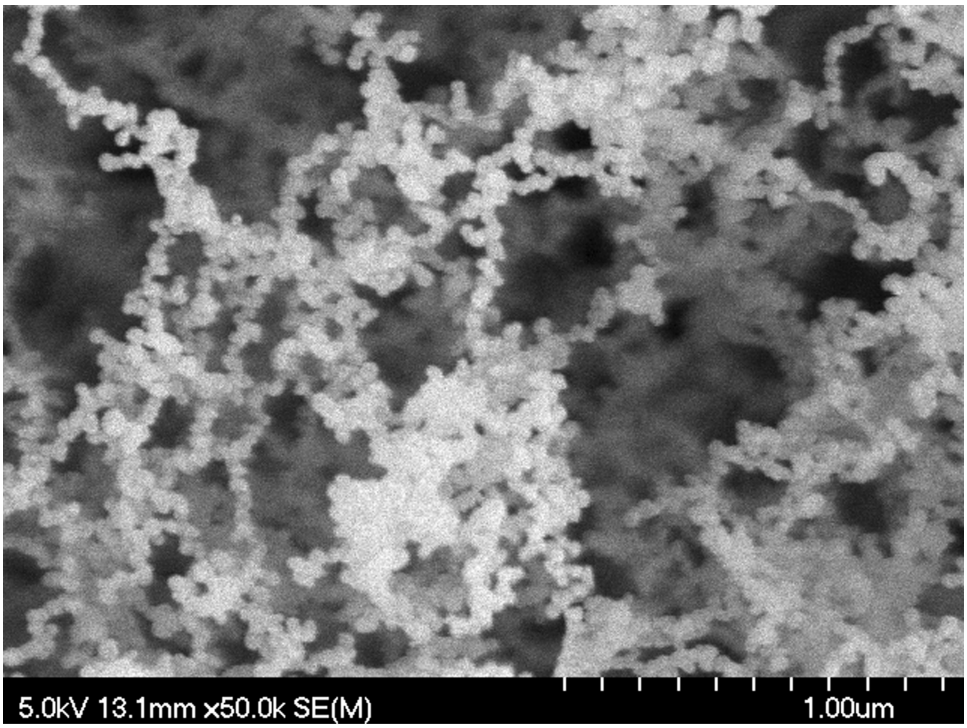

(c)

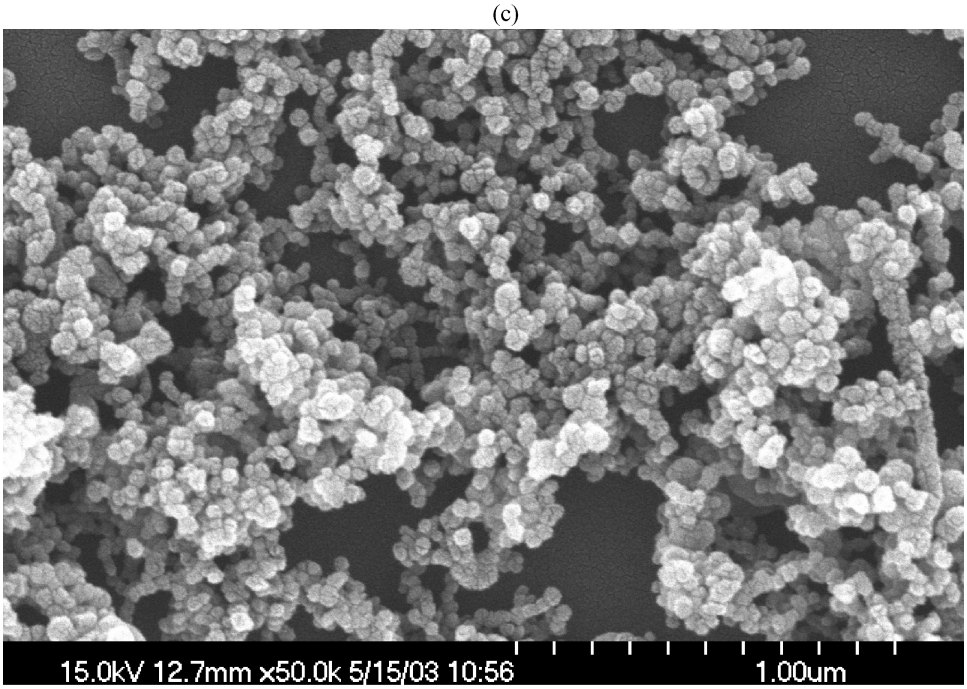

(d)

FIG. 2. (Continued)

3. RESULTS AND DISCUSSION

3.1 Effect of Applied Voltage

For the study of the effect of applied voltage on the size distribution of generated particles, the TTIP/H_2O precursor molar ratio was 11.9 as bubbled at the temperature of 150°C and the frequency was 60 Hz in the aerosol generator. Figures 2a–d show the SEM photo images of the particles generated at applied voltage of 0, 6.48, 8.58, and 9.60 kV, respectively. It was observed that the generated particles were in a broad size distribution as no

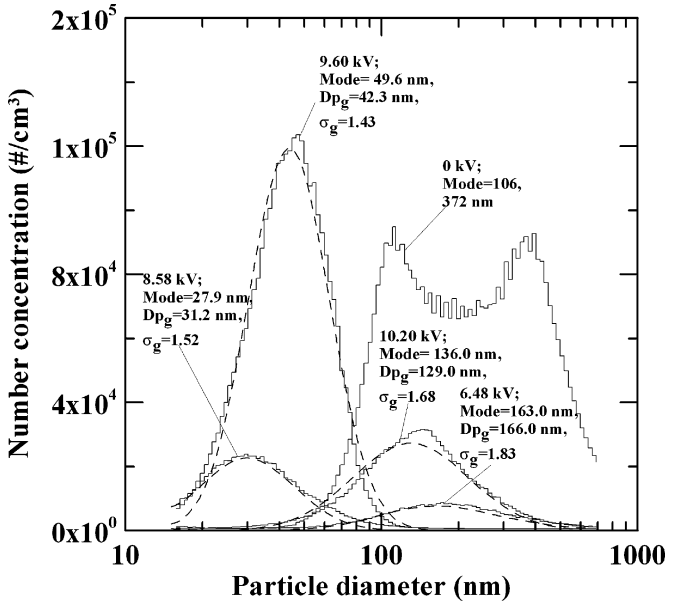

FIG. 3. Particle size distributions measured by SMPS after dilution ratio of 1. The operation condition was the same as that of Figure 2. Step-lines are SMPS measured data obtained at different applied voltages, and dash-lines are their lognormal fittings.

voltage was applied, the particle sizes could be as large as 1 μm or smaller than 100 nm. On the other hand, as the voltage was applied the particle sizes became smaller and more uniformly distributed.

The SMPS on-line measurement data for the particle size distribution are shown in Figure 3. The experimental conditions for the APPENS reactor were the same as that shown in Figure 2. As no voltage was applied, the TiO_2 particles show bi-modal distribution with two mode sizes at around 106 nm and 372 nm, respectively. And the particle size appears to be uni-modal distributed as the voltage was applied. The mode of particle size decreases from 163 nm to 27.9 nm as increasing the applied voltage from 6.48 to 8.58 kV. But further increases in the values of applied voltage to 9.60 and 10.20 kV result in increases in the mode size instead. The lognormal fittings (dashed-lines) seem to obtain good correlation with the SMPS online measurement data (step-lines) for the plasma produced particles. The calculated values of σ_g ranged from 1.43 to 1.83 for particles generated at the applied voltage of 6.48 to 10.20 kV.

Values of Dp_g of generated particles at applied voltage of 6.48, 8.58, 9.60, and 10.20 kV were also determined from the SEM images and they were 75, 31, 39, and 43 nm, respectively, with their corresponding values of σ_g of 1.5, 1.2, 1.4, and 1.3. By comparing values of Dp_g and σ_g determined from the SEM images to those from SMPS data, one can see that particle sizes measured by the SMPS were larger and the distribution were broader. This is opposite to those predicted by the diffusion and electrostatic mechanisms that particles deposited on the reactor wall should have broader size distribution than those penetrating the reactor. The larger Dp_g and σ_g of particles penetrating the reactor may be mainly caused by that loosely agglomerated particles were counted by the SMPS as one single particle. This is confirmed by that values of σ_g measured by the SMPS (shown in Figure 3) are larger than the value predicted by the self preserving size distribution theory for coagulating spheres, 1.33 (Vemury et al. 1994). Larger values of σ_g are typically the result of particle agglomeration without coalescence in the gas phase.

Nakaso et al. (2003) indicated that faster reaction rate of TTIP conversion led to narrow particle size distribution. In this study, the TTIP conversion rate is enhanced by applying the plasma in this system. In addition, the non-thermal plasma kept the gas temperatures to be low within and after the aerosol generator. This particular condition is similar to the effect of cooling gas which can restrain the coalescence between the particles (Joshi et al. 1990; Tsantilis and Pratsinis 2004b). On the contrary of without applying any voltage or at low applied voltage, the bimodal size distribution or broad distribution may be due to the slow reaction rate of precursors or particles (Nakaso et al. 2003; Kuster and Pratsinis 1995; Ahonen et al. 1999). Thus the application of plasma not only avoids the further coalescence of the agglomerated particles, but also enhances the hydration rate of the precursors. But if the applied voltage is increased to be too strong ($\sim$10.2 kV), the melting possibility of smaller particles in the agglomerates is increased. This leads to larger product particles or hard agglomerates of small particles. Hence the optimal applied voltage is 9.6 kV for better production of catalytic particles with nanosize distribution, high production yield and less agglomeration.

3.2 Effect of Electric Frequency

The effects of electric frequency at 60, 120, and 240 Hz on the morphology and size distribution of particles were investigated by the SEM and SMPS analyses and results are shown in Figure 4. The applied voltage was 10.20 kV and the TTIP/H_2O precursor molar ratio was 11.9 by bubbling of the TTIP at 150°C. A very interesting phenomenon was observed from the SMPS data that as increasing the frequency from 60 Hz to 240 Hz, the particle concentration decreases significantly. The SMPS distributions in Figure 4 for the 120 Hz and 240 Hz are so low in concentration that they may not be representative of the actual size distribution of the particles produced.

The SEM morphology of particles deposited in the reactor which generated at 240 Hz was very different from those at 60 and 120 Hz as seen from Figure 4. The particles seemed to develop a film at 240 Hz. The approximate sizes of particles from SEM images for 60 and 120 Hz are 43 and 34 nm, respectively. But the particle sizes of 240 Hz were difficult to calculate from this SEM image due to its film structure. This result is similar to literature data on the SiO_2 thin film (Thyen et al. 1997; Foest et al. 2003) deposited at high frequency (20–100 KHz). Therefore, most of the precursor vapors deposited in the plasma reactor and formed a thin film at frequency of 240 Hz. This may explain why

Downloaded by [National Chiao Tung University] at 00:37 26 April 2014

Downloaded by [National Chiao Tung University] at 00:37 26 April 2014

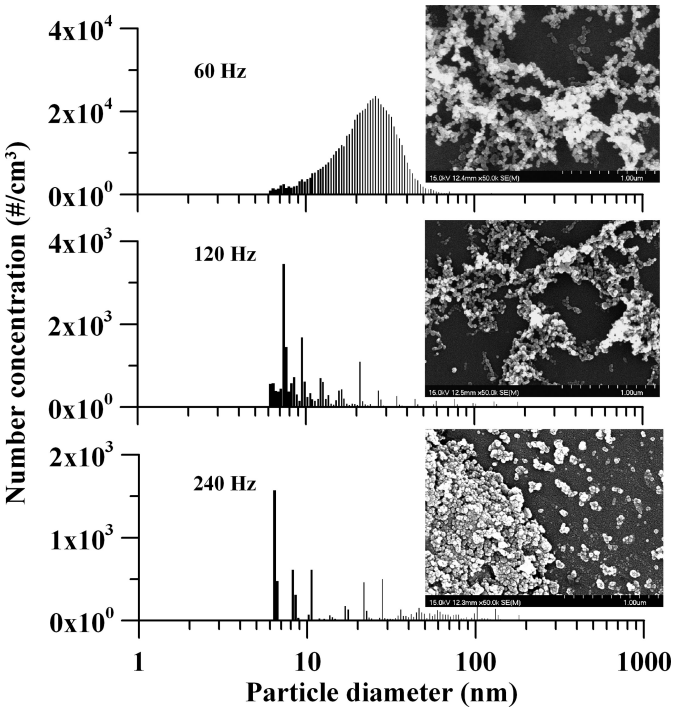

FIG. 4. Particle size distributions measured by SMPS after dilution ratio of 12 under different electric frequencies. Also shown are SEM images of the reactor-deposited particles. The applied voltage was 10.20 kV, the TTIP/H_2O precursor molar ratio was 11.9 as TTIP bubbled at 150°C.

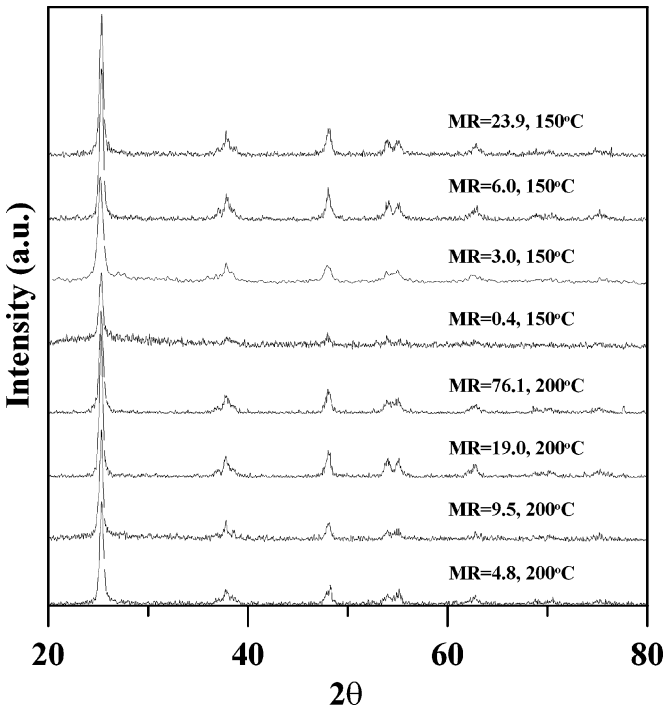

FIG. 5. The XRPD patterns of generated particles synthesized in this study. The operation condition was the same as that of Table 1 with TTIP/H_2O precursor molar ratio (MR) from 0.4 to 76.1 and TTIP bubbling temperature of 150 or 200°C.

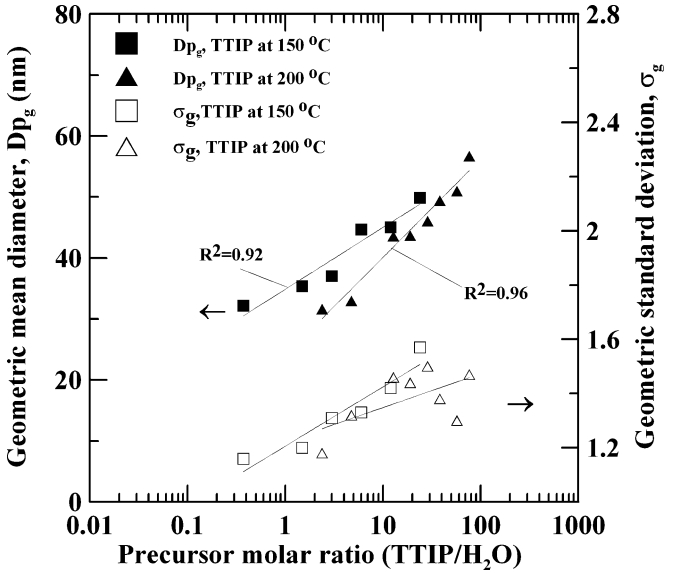

FIG. 6. Effect of precursor molar ratio on the size distributions of particles collected in the reactor and measured by SEM images. The applied voltage was 9.60 kV and the TTIP bubbling temperatures were at 150 or 200°C.

a lower particle concentration was measured after the reactor by SMPS as the applied frequency was increased. As a result, the APPENS could work as an aerosol generator at lower frequency of 60 Hz. And it can also be applied for producing thin film at higher frequency of 240 Hz. But for a frequency of 120 Hz, the SMPS detected too low particle concentration while the SEM did not observe a nice film developed so it maybe applied for neither purpose.

3.3 Effect of Precursor Molar Ratio

The crystalline phase of generated particles was determined with the XRPD pattern and the results are shown in Figure 5. The XRPD peaks at around 25°, 38°, 48°, 55°, and 63° corresponding to anatase crystal are observed for all synthesized samples, with the most significant peak at around 25°. And the peak intensities at all angles seem to be increased with increasing the molar ratio. The effect of TTIP/H_2O precursor molar ratios on the crystalline sizes of particles was estimated from XRPD data by Scherrer equation (Musić et al. 1997),

$$D = \frac{0.9\lambda}{\beta \cos\theta}$$

where D (nm) is the crystalline size, λ (nm) is X-ray wavelength for the XRPD tests, θ is Bragg angle, and β is full width of diffraction at half of maximum intensity (FWHM). The calculated crystalline sizes are listed in Table 1. As seen in Table 1, the average crystalline size of particles generated at TTIP bubbling temperature of 200° is around 23.5 ± 2.4 nm, which is slightly larger than the value of 22.2 ± 1.1 nm at 150°C. And the average of all data is 22.8 ± 2.0 nm. The data are within the

TABLE 1
Crystalline size of TiO_2 particles generated via different TTIP/H_2O precursor molar ratios. The crystalline sizes of primary particle were calculated based on Scherrer equation with parameter values obtained from XRPD patterns at X-ray wavelength (λ) of 0.154056 nm.

TTIP bubbling temperature (°C)	Flow ratio (TTIP/H_2O)	Molar ratio (TTIP/H_2O)	FWHM	2θ (degree)	Crystalline size (nm)
150	8	23.9	0.0064	25.33	22.2
150	2	6.0	0.0067	25.33	21.3
150	1	3.0	0.0065	25.28	21.8
150	0.125	0.4	0.0061	25.36	23.3
150	Average size	–	–	–	22.2 ± 1.1
200	4	76.1	0.0067	25.31	21.1
200	1	19.0	0.0057	25.29	24.8
200	0.5	9.5	0.0058	25.30	24.5
200	0.25	4.8	0.0061	25.35	23.5
200	Average size	–	–	–	23.5 ± 2.4
	Total average size	–	–	–	22.8 ± 2.0

Downloaded by [National Chiao Tung University] at 00:37 26 April 2014

experimental error and thus one can say that the effect of molar ratio on crystalline sizes of particles is not significant.

The primary particle can be composed of more than one crystal or can be partly crystalline and contain some amorphous TiO_2. The effect of precursor molar ratio on the primary particle size is also evaluated via averaging over 80 particles in the SEM imagines for each test condition. The results are shown in Figure 6 with symbols indicate the SEM averaged size distribution data and lines are logarithmic regression results of Dp_g and σ_g with respect to the precursor molar ratio.

One can see in Figure 6 that decreasing the precursor molar ratio results in a smaller and uniform particle size. Based on the regression curves, Dp_g of particles is decreased from around 60 nm to 30 nm and σ_g of particle distribution is decreased from 1.6 to 1.2 as decreasing the TTIP/H_2O precursor molar ratio from 76.1 to 0.4. The precursor molar ratio has a slightly stronger effect on Dp_g at TTIP bubbling temperature of 200°C. But values of σ_g for data obtained at 200°C do not seem to be increased further as increasing the TTIP/H_2O molar ratio. It must be noted that at very low TTIP/H_2O precursor molar ratio the generated particle number concentration is much lower. Hence the decreasing of σ_g to monodisperse aerosol by decreasing TTIP/H_2O precursor molar ratio is accompanied by that less particles are generated. This may not be acceptable for some particle generation application.

To further verify the precursor effect on the particle size distribution, TEM images were also taken and shown in Figures 7(a) and (b), respectively, for TTIP/H_2O precursor molar ratios of 1.1 and 76.1. The TEM images reveal similar trend to the SEM observed data shown in Figure 6 that increasing the precursor concentration leads to a broader size distribution. At a low TTIP/H_2O precursor molar ratio of 1.1, the particle sizes are near uniform with size of around 30–40 nm. From Figure 6 one knows that at TTIP/H_2O precursor molar ratio of 1.1 and TTIP bubbling temperature of 150°, value of Dp_g is around 35 nm and σ_g is around 1.2. Based on the lognormal distribution, 95% of the particles for such a size distribution should fall within 29 and 42 nm. This size range corresponds well with the TEM observation shown in Figure 7(a). But at a high TTIP/H_2O precursor molar ratio of 76.1, the TEM observed a much broader particle size distribution with particle size ranges from around 15 to 80 nm.

The observation that higher precursor concentration leads to higher particle size distribution seems to be opposite to the TiO_2 thermo-decomposition result of Pratsinis and Spicer (1998), where surface reaction is the dominating mechanism for the change of particle size distribution. This can be explained by that the hydrolysis reaction of TTIP with H_2O is much faster than the thermo-decomposition rate of TTIP (Okuyama et al. 1990; Seto et al. 1995). Thus hydrolysis reaction is the dominating mechanism for the formation of TiO_2 particles at low TTIP/H_2O molar ratio, thus the particle size distribution is narrower. On the other hand, at high TTIP/H_2O molar ratio (above the stoichiometric ratio of hydrolysis reaction) the formation of TiO_2 particles was first induced by hydrolysis reaction, then excess of TTIP forms TiO_2 monomers by thermo-decomposition mechanism, and the monomers either nucleate as new particles or condense onto the TiO_2 particles which were previously formed by hydrolysis reaction. As a result, the particle size distribution is broader at high TTIP/H_2O precursor molar ratio due to both hydrolysis and thermo-decomposition reactions occurred for the formation of TiO_2 particles.

3.4 Long-Term Stability

The size distributions of particles generated from APPENS reactor were measured continuously by SMPS for 1 hr to test the long-term stability of the aerosol generator, and variations

Downloaded by [National Chiao Tung University] at 00:37 26 April 2014

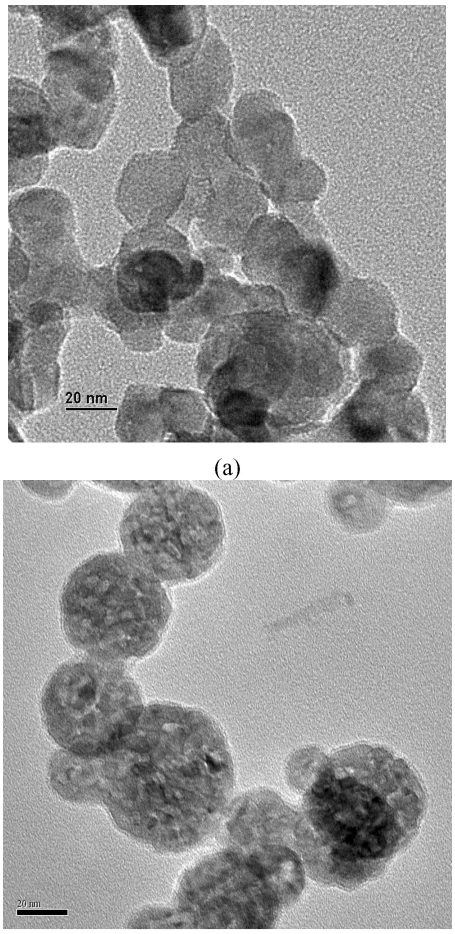

FIG. 7. TEM images (scale bar = 20 nm) of particles collected in the reactor as obtained at two different TTIP/H_2O precursor ratios of 1.1 and 76.1, respectively. The applied voltage was 9.60 kV and the TTIP bubbling temperatures were at 150 and 200°C, respectively. The low TTIP/H_2O precursor ratio of 1.1 clearly indicates higher uniformity of TiO_2 particles.

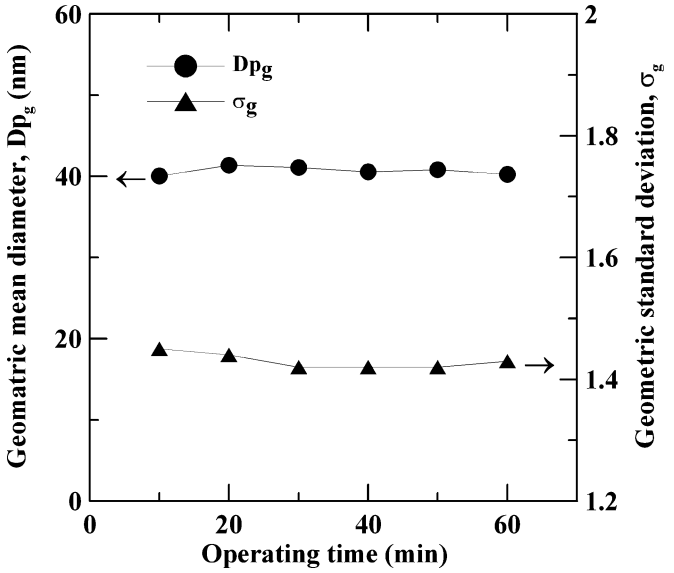

FIG. 8. Stability of geometric mean particle diameter (Dp_g) and geometric standard deviation (σ_g) measured by SMPS during one hour of operation time. The frequency was 60 Hz, the TTIP/H_2O molar ratio was 0.7 as TTIP bubbled at 150°C and the applied voltage was 9.60 kV.

of Dp_g and σ_g with respect to time are shown in Figure 8. The generator was operated under conditions of TTIP/H_2O precursor molar ratio of 0.7 (with TTIP bubbled at 150°C), applied voltage of 9.60 kV, frequency of 60 Hz and without any dilution. The average value of Dp_g of generated particles is 40.7 ± 0.5 and σ_g of them is 1.43 ± 0.1. The result indicated that the particle size distribution is stable and the APPENS generator can be used for long-term operation.

3.5 Comparison of APPENS Generator with Commercial Aerosol Generators

Table 2 compares the properties of particles generated via the APPENS generator to the furnace reactor as well as to commercial nano-size range (<100 nm) aerosol generators. Both the APPENS and the furnace reactor produce particles via chemical process of gas to particle conversion. The furnace reactor produces TiO_2 particles at high temperature via thermo-decomposition mechanism and the particle number concentration is very high (10^{10} #/cm^3) with σ_g of around 1.3–1.5. The APPENS generator is operated at room temperature and it produces TiO_2 particles via hydrolysis and thermo-decomposition mechanisms. It is capable of generating particles with number concentration of around 10^6 #/cm^3 and σ_g of around 1.2 to 1.5.

As for the commercial aerosol generators, the electrospray aerosol generator is a monodisperse nanoparticle generator, while the atomizer and the spark aerosol generators generate polydisperse particles. The generated particles from both atomizer and spark aerosol generator (GFG-1000) are in a broad size range ($\sigma_g > 1.6$) and thus classifiers are needed to produce monodisperse nanoparticles. the electrospray aerosol generator produces particles from the charged solution through the capillary by electrical field pulling. The atomizer atomizes liquid particles through an orifice by high-velocity jet. The spark aerosol generator (GFG-1000) uses high voltage to generate sparks between two graphite electrodes and forms graphite fine particles by evaporation-condensation mechanism. The morphologies of generated solid particles were spherical via APPENS and furnace reactor. The electrospray and atomizer can also generate spherical liquid aerosol, but they are difficult to generate solid spherical particles. The spark aerosol generator (GFG-1000) can generate either metals or graphite particles.

4. CONCLUSION

The effects of applied voltage, frequency, and the precursor molar ratio on particle morphology and particle size distributions

TABLE 2
Comparison of the APPENS generator with commercial aerosol generators. Only nano-size (<100 nm) aerosol generators are included

Aerosol generator	Particle Generation Mechanism	Size range (nm)	σ_g	Total concentration (#/cm^3)	Morphology/ Component of generated particles
This study (APPENS)	Nonthermal plasma/ hydrolysis& thermal decomposition	<10–100 (with controllable average size ranges from 30–60)	1.2–1.5	10^6	Loose agglomerates of spherical primary particles (solid phase)/ TiO_2 at the present time
Furnace reactor (Nakaso et al. 2001)	High temperature flame/ Thermal decomposition	12–17[c]	1.3–1.5	10^{10}	Spherical/ TiO_2
		4–8[d]	1.3–1.5	10^{10}–10^{11}	
Electrospray Aerosol Generator; 3480[a]	Electrical field spray	2–100	1.1	10^7	Spherical (liquid phase)/ Soluble solids or nonvolatile liquids
Aerosol generator; GFG-1000[b]	Spark	20–150	>1.6	10^7	Nature soot liked/ Graphite, metals
Constant Output Atomizer; 3076, 3079, 9302 & 9306A[a].	High velocity jet atomizing	10–2,000	>1.6	10^7	Spherical/ PSL[e], DOP[f], oils, and other aqueous or alcohol solutions or suspensions
		10–2,000	>1.6	10^8	Spherical/ DEHS[g], DOP, Emery 3004, Paraffines, PSL, Salt solutions
		10–2,000	>1.6	10^7	Spherical/ Water-soluble materials (salt or sugar)
		10–2,000	<2.0	10^7	Spherical/ PSL, DOP, DEHS, oils, and other aqueous or alcohol solutions or suspensions

[a]TSI Inc.
[b]PALAS® Aerosltechnologie aerosol technology.
[c]TTIP precursor.
[d]$TiCl_4$ precursor.
[e]PSL: Polystyrene latex.
[f]DOP: Di-octyl phthalate.
[g]DEHS: Di-ethyl-hexyl-sebacin acid.

Downloaded by [National Chiao Tung University] at 00:37 26 April 2014

were described in this study. The APPENS generator can produce nanoparticles of uni-modal size distributions. It is concluded that the APPENS process has a high potential to be used as a size controllable monodisperse or polydisperse aerosol generator. The APPENS generator is simple to be composed of and it can be scaled up by using several more parallel tubes to enlarge the production rate (Lin and Bai 2001) as already approached for a commercial O_3 generator. As a result, the APPENS process could be utilized for the purpose of either implication or application studies of TiO_2 nanoparticles. Further research work might also be extended to generate other chemical components of nanoparticles such as SiO_2, ZnO, and MgO.

REFERENCES

Ahonen, P. P., Kauppinen, E. I., Joubert, J. C., Deschanvres, J. L., and Tendeloo, G. V. (1999). Preparation of Nanocrystalline Titan Powder via Aerosol Pyrolysis of Titanium Tetrabutoxide. *J. Mater. Res*. 14:3938–3948.

Downloaded by [National Chiao Tung University] at 00:37 26 April 2014

Almquist, C. B., and Biswas, P. (2002). Role of synthesis method and particle size of nanostructured TiO_2 on its photoactivity, *J. Catal.* 212:145–156.

Arabi-Katbi, O. I., Pratsinis, S. E., Morrision, P. W., Jr., and Megaridis, C. M. (2001). Monitoring the Flame Synthesis of TiO_2 Particles by in-situ FTIR Spectroscopy and Thermophoretic Sampling, *Comb. Flame*. 124:560–572.

Bai, H., Chen, C., Lin, C.-H., Den, W., and Chang, C. (2004). Monodisperse Nanoparticle Synthesis by an Atmospheric Pressure Plasma Process: An Example of a Visible Light Photocatalyst, *Ind. Eng. Chem. Res*. 43:7200–7203.

Berglund, R. N., and Liu, B. Y. H. (1997). Generation of Monodisperse Aerosol Standards, *Environ. Sci. Technol*. 7(2):147–153.

Chang, M. B., Kushner, M. J., and Rood, M. J. (1992). Gas Phase Removal of NO from Gas Stream via Dielectric Barrier Discharges, *Environ. Sci. Technol*. 26(4):777–781.

Chein, H.-M., and Lundgren, D. A. (1995). A High-output, Size-selective Aerosol Generator, *Aerosol Sci. Technol*. 23:510–520.

Chen, C., Bai, H., Chang, S.-M., Chang, C., and Den, W. (2007). Preparation of N-doped TiO_2 Photocatalyst by Atmospheric Pressure Plasma Process for VOCs Decomposition under UV and Visible Light Sources, *J. Nanoparticle Res*. 9:365–375.

Chen, D.-R., Pui, D. Y. H., and Kaufman, S. L. (1995). Electrospraying of Conducting Liquids for Monodisperse Aerosol Generation in the 4 nm to 1.8 μm Diameter Range, *J. Aerosol Sci*. 26:963–977.

Cho, K., and Biswas, P. (2006). Sintering Rates for Pristine and Doped Titanium Dioxide Determined Using a Tandem Differential Mobility Analyzer System, *Aerosol Sci. Technol.* 40:309–319.

Duminica, F.-D., Maury, F., and Senocq, F. (2004). Atmospheric Pressure MOCVD of TiO_2 Thin Films Using Various Reactive Gas Mixtures, *Surf. Coat. Technol.* 188–189:255–259.

Evans, D. E., Harrison, R. M., and Ayres, Je G. (2003). The Generation and Characterization of Metallic and Mixed Element Aerosols for Human Challenge Studies, *Aerosol Sci. Technol*. 37:975–987.

Foest, R., Adler, F., Sigeneger, F., and Schmidt, M. (2003). Study of an Atmospheric Pressure Glow Discharge (APG) for Thin Film Deposition, *Surf. Coat. Technol*. 163–164:323–330.

Friedlander, S. K. (2000). *Smoke, Dust and Haze: Fundamentals of Aerosol Dynamics*, 2nd ed., pg. 217, Oxford University Press, USA.

Fujishima, A., Rao, T. N., and Tryk, D. A. (2000). Titanium Dioxide Photocatalysis, *J. Photochem. Photobiol. C: Photochem. Rev*. 1:1–21.

Hoffmann, M. R., Martin, S. T., Choi, W., and Bahnemannt, D. W. (1995). Environmental Applications of Semiconductor Photocatalysis, *Chem. Rev*. 95:69–96.

Horvath, H., and Gangl, G. (2003). A Low-Voltage Spark Generator for Production of Carbon Particles, *J. Aerosol Sci*. 34:1581–1588.

Joshi, S. V., Liang, Q., Park, J. Y., and Batdorf, J. A. (1990). Effect of Quenching Conditions on Particle Formation and Growth in Thermal Plasma Synthesis of Fine Powders, *Plasma Chem. Plasma Process*. 10(2):339–358.

Kim. C. S., Nakaso, K., Xia, B., Okuyama, K., and Shimada, M. (2005). A New Observation on the Phase Transformation of TiO_2 Nanoparticles Produced by a CVD Method, *Aerosol Sci. Technol*. 39:104–112.

Kim, D.-J., Kim, K.-S., and Zhao, Q.-Q. (2003). Production of Monodisperse Nanoparticles and Application of Discrete–monodisperse Model in Plasma Reactors, *J. Nanoparticle Res.* 5:211–223.

Kulkarni, P., Namiki, N., Otani, Y., and Biswas, P. (2002). Charging of Particles in Unipolar Coronas Irradiated by In-situ Soft X-rays: Enhancement of Capture Efficiency of Ultrafine Particles, *J. Aerosol Sci.* 33:1279–1296.

Kusters, K. A., and Pratsinis S. E. (1995). Strategies for Control of Ceramic Powder Synthesis by Gas-to-Particle Conversion, *Powder Technol*. 82:79–91.

Lee, D., and Choi, M. (2002). Coalescence Enhanced synthesis of Nanoparticles to Control Size, Morphology and Crystalline Phase at High Concentrations, *J. Aerosol Sci*. 33:1–16.

Lin, C.–H., and Bai, H. (2001). Energy-Effectiveness of Non-Thermal Plasma Reactors for Toluene Vapor Destruction, *ASCE J. Environ. eng*. 127(7):648–654.

Martin, S., Massines, F., Gherardi, N., and Jimenez, C. (2004). Atmospheric Pressure PE-CVD of Silicon Based Coatings Using a Glow Dielectric Barrier discharge, *Surf. Coat. Technol*. 177–178:693–698.

Musić S., Gotić, M., Ivanda, M., Popvić, S., Turković, A., Trojko, R., Sekulić, A., and Furić, K. (1997). Chemical and Microstructural Properties of TiO_2 Synthesized by Sol-Gel Procedure, *Mater. Sci. Eng. B*. 47:33–40.

Nakade, S., Matsuda, M., Kambe, S. Saito, Y. Kitamura, T., Sakata, T., Wada, Y., Mori, H., and Yanagida, S. (2002). Dependence of TiO_2 Nanoparticle Preparation Methods and Annealing Temperature on the Efficiency of Dye-Sensitized Solar Cells, *J. Phys. Chem. B*. 106:10004–10010.

Nakaso, K., Okuyama, K., Shimada, M., and Pratsinis, S. E. (2003). Effect of Reaction Temperature on CVD-Made TiO_2 Primary Particle Diameter, *Chem. Eng. Sci*. 58:3327–3335.

Nakaso, K., Fujimoto, T., Seto, T., Shimada, M., Okuyama, K., and Lunden, M. M. (2001). Size Distribution Change of Titania Nano-particle Agglomerates Generated by Gas Phase Reaction, Agglomeration, and Sintering, *Aerosol Sci. Technol.* 35:929–947.

Okuyama, K., Kousaka, Y., Tohge, N., Yamamoto, S., Wu, J. J., Flagan, R. C., and Seinfeld, J. H. (1986). Production of Ultrafine Metal Oxide Aerosol Particles by Thermal Decomposition of Metal Alkoxide Vapors, *AIChE J.* 32:2010–2019.

Okuyama, K., Ushio, R., Kousaka, Y., Flagan, R. C., and Seinfeld, J. H. (1990). Particle Generation in a Chemical Vapor Deposition Process with Seed Particles, *A.I.Ch.E. Journal*. 36:409–419.

Park, K. Y., Ullmann, M., Suh, Y. J., and Friedlander, S. K. (2001). Nanoparticle Microreactor: Application to Synthesis of Titania by Thermal Decomposition of Titanium Tetraisopropoxide, *J. Nanoparticle Res*. 3:309–319.

Pratsinis, S. E., Zhu, W., and Vemury, S. (1996). The Role of Gas Mixing in Flame Synthesis of Titania Powder, *Powder Technol*. 87:87–93.

Pratsinis, S. E., and Spicer, P. T. (1998). Competition Between Gas Phase and Surface Oxidation of $TiCl_4$ during Synthesis of TiO_2 Particles, *Chem. Eng. Sci.* 53, 10:1861–1868.

Peinekea, C., Attouib, M. B., and Schmidt-Otta, A. (2006). Using a Glowing Wire Generator for Production of Charged, Uniformly Sized Nanoparticles at High Concentrations, *J. Aerosol Sci*. 37:1651–1661.

Prenni, A. J., Siefert, R. L., Onasch, T. B., Tolbert, M. A., and DeMott, P. J. (2000). Design and Characterization of a Fluidized Bed Aerosol Generator: A Source for Dry, Submicrometer Aerosol, *Aerosol Sci. Technol*. 32:465–481.

Seto, T., Shimada, M., and Okuyama, K. (1995). Evaluation of Sintering of Nanometer-Sized Titania Using Aerosol Method, *Aerosol Sci. Technol*. 23:183–200.

Spicer, P. T., Chaoul, O., Tsantilis, S., and Pratsinis, S. E. (2002). Titania Formation by $TiCl_4$ Gas Phase Oxidation, Surface Growth and Coagulation, *J. Aerosol Sci*. 33:17–34.

Thyen, R., Weber, A., and Klages, C.-P. (1997). Plasma-enhanced Chemical-vapor-Deposition of Thin Films by Corona Discharge at Atmospheric Pressure, *Surf. Coat. Technol*. 97:426–434.

Tsantilis, S., Kammler, H. K., and Pratsinis S. E. (2002). Population Balance Modeling of Flame Synthesis of Titania Nanoparticles, *Chem. Eng. Sci*. 57:2139–2156.

Tsantilis, S., and Pratsinis, S. E. (2004a). Narrowing the Size Distribution of Aerosol-Made Titania by Surface Growth and Coagulation, *J. Aerosol Sci*. 35:405–420.

Tsantilis, S., and Pratsinis, S. E. (2004b). Soft- and Hard-agglomerate Aerosols Made at High Temperatures, *Langmuir*. 20:5933–5939.

Vemury, S., Kusters, K. A., and Pratsinis, S. E. (1994). Time-Lag for Attainment of the Self-Preserving Particle-Size Distribution by Coagulation, *J. Colloid Interface Sci.* 165, 1:53–59.

Veranth, J. M., Gelein, R., and OberdÖrster, G. (2003). Vaporization-condensation Generation of Ultrafine Hydrocarbon Particulate Matter for Inhalation Toxicology Studies, *Aerosol Sci. Technol*. 37:603–609.

Wang, Z.-M., Yang, G., Biswas, P., Bresser, W., and Boolchand, P. (2001). Processing of Iron-doped Titania Powders in Flame Aerosol Reactors, *Powder Technol.* 114:197–204.

Yang, G., Zhuang, H., and Biswas, P. (1996). Characterization and Sinterability of Nanophase Titania Particles Processed in Flame Reactors, *NanoStructured Mater.* 7, 6:675–689.

Zimmer, A. T., Baron, P. A., and Biswas, P. (2002). The Influence of Operating Parameters on Number-Weighted Aerosol Size Distribution Generated from a Gas Metal Arc Welding Process, *J. Aerosol. Sci.* 33:519–531.

Downloaded by [National Chiao Tung University] at 00:37 26 April 2014